

the Planck 2018 final analysis [19], and the BAO data from the measurements of 6dFGS survey[20], SDSS DR7 MGS[21], and BOSS DR12[22].

This paper is organized as follows. In Section 2, we briefly introduce the phenomenological model under consideration. The Section 3 presents the observational data adopted in this work. The results from observational constraints and the corresponding analyses are displayed in Section 4. In the last section, we summarize the main conclusions.

2. Phenomenological model: basic equations

The model under consideration is characterized with a phenomenological form for the ratio of the dark energy and matter densities [12, 13],

$$\rho_X \propto \rho_m a^\xi, \quad \text{or} \quad \Omega_X \propto \Omega_m a^\xi, \quad (1)$$

where Ω_X and Ω_m are the fractions of the energy density of the universe contributed from dark energy and matter, respectively. The scaling parameter ξ can be constrained from observational data and used to reveal the severity of the coincidence problem.

Considering a flat FLRW universe with $\Omega_X + \Omega_m = 1$, we can obtain

$$\Omega_X = \frac{\Omega_{X,0} a^\xi}{1 - \Omega_{X,0} (1 - a^\xi)}, \quad (2)$$

where $\Omega_{X,0} = \Omega_X(z=0)$. According to the energy conservation equation, we have

$$\frac{d\rho_{\text{tot}}}{da} + \frac{3}{a} (1 + \omega_X \Omega_X) \rho_{\text{tot}} = 0, \quad (3)$$

where $\rho_{\text{tot}} = \rho_m + \rho_X$ is the total energy density, ω_X specifies the equation of state of the dark energy. Meanwhile, the Eq.(3) can be rewritten as

$$\frac{d\rho_m}{da} + \frac{3}{a} \rho_m = - \left[\frac{d\rho_X}{da} + \frac{3}{a} (1 + \omega_X) \rho_X \right] = Q, \quad (4)$$

where $Q = -(\xi + 3\omega_X)\rho_m \kappa a^{\xi-1}/(1 + \kappa a^\xi)$ and $\kappa = \rho_X/(\rho_m a^\xi)$, and the interaction term $Q = 0$ ($\neq 0$) denotes the cosmology without (with) interaction between dark energy and matter.

Based on Eq.(3), we can work out

$$\frac{\rho_{\text{tot}}}{\rho_0} = \exp\left(\int_a^1 \frac{da}{a} 3(1 + \omega_X \Omega_X)\right). \quad (5)$$

Assuming ω_X as a constant, we can rewritten the above equation as

$$E^2(z) = \exp\left(\int_a^1 \frac{da}{a} 3(1 + \omega_X \Omega_X)\right), \quad (6)$$

where $E^2(z) \equiv [H(z)/H_0]^2 = \rho_{\text{tot}}/\rho_0$, and $E(z)$ is the dimensionless Hubble parameter. When $\xi = \text{Constant}$, we can solve Eq.(6) and get

$$E^2(z; \mathbf{p}) = a^{-3} \left(1 - \Omega_{X,0} (1 - a^\xi)\right)^{-3\omega_X/\xi}, \quad (7)$$

where the parameter set is $\mathbf{p} \equiv (\Omega_{X,0}, \omega_X, \xi)$. However, for a variable $\xi(z)$,

$$\xi(z) = \xi_0 + \xi_z * \frac{z}{1+z}.$$

We cannot obtain the analytical solution of Eq.(6). Then we should solve it numerically with the parameter set $\mathbf{p} \equiv (\Omega_{X,0}, \omega_X, \xi_0, \xi_z)$.

3. Data sample

The observational data sets used in our cosmological analyses are described as follows, including the Pantheon SNe Ia sample, the CMB power spectrum data from the final Planck 2018 results, and the BAO data from the 6dFGS survey, the SDSS DR7 MGS, and the BOSS DR12 measurements.

3.1. SNe Ia data set

The SNe Ia as standard candles have been proved to be a kind of sensitive probe of cosmology (see, e.g. [23, 24, 25]). The population of confirmed SNe Ia has a dramatic increase over the last two decades, in the mean time, the techniques for measuring the light curve parameters are also continually being improved to reduce the systematic uncertainties. At present, the most popular techniques mainly include the SALT/SALT2 [26, 27] and SiFTO [28] models, which are two popular techniques at present and fit the light curves of SNe Ia by using the spectral template.

The SNe Ia sample adopted in this work is the Pantheon sample [18], which consists of 1048 SNe Ia ($0.01 \leq z \leq 2.3$) combined from Pan-STARRS1(PS1) Medium Deep Survey, SDSS, SNLS, various low- z and HST samples. In the Pantheon sample, the distances for each of these SNe Ia are determined after fitting their light-curves with the most up-to-date published version of SALT2 [29], then applying the BEAMS with Bias Corrections (BBC) method [30] to determine the nuisance parameters and adding the distance bias corrections. The uniform analysis procedure conducted on the SNe Ia of Pantheon sample has significantly reduced the systematic uncertainties related to photometric calibration.

The observable given in the Pantheon sample can be deemed as a correction to the apparent magnitude (see Table A17 of [18]), i.e.,

$$\begin{aligned} Y^{obs} &= m_B + K \\ &= \mu + M, \end{aligned} \quad (8)$$

where μ is the distance modulus, m_B is the apparent B-band magnitude, M is the absolute B-band magnitude of a fiducial SN Ia, and the correction term $K = \alpha x_1 - \beta c + \Delta_M + \Delta_B$ includes the corrections related to four different sources (see [18] for more details). The corresponding theoretical (predicted) value is

$$\begin{aligned} Y^{th} &= 5 \log(d_L) + 25 + M \\ &= 5 \log[(1+z)D(z)] + Y_0, \end{aligned} \quad (9)$$

Table 1: The BAO data adopted in this work.

Survey	z_{eff}	Measurement	Value	σ
6dFGS	0.106	r_s/D_V	0.336	0.015
SDSS DR7 MGS	0.15	$D_V(r_{s,\text{fid}}/r_s)$	664	25
BOSS DR12	0.38	$D_M(r_{s,\text{fid}}/r_s)$	1518	–
	0.38	$H(z)(r_s/r_{s,\text{fid}})$	81.5	–
	0.51	$D_M(r_{s,\text{fid}}/r_s)$	1977	–
	0.51	$H(z)(r_s/r_{s,\text{fid}})$	90.4	–
	0.61	$D_M(r_{s,\text{fid}}/r_s)$	2283	–
	0.61	$H(z)(r_s/r_{s,\text{fid}})$	97.3	–

where the constant term Y_0 is written as $Y_0 = M + 5\log(\frac{cH_0^{-1}}{\text{Mpc}}) + 25$, and the luminosity distance d_L and the normalized comoving distance $D(z)$ are related with each other through the following formula, i.e.,

$$d_L(z) = \frac{c(1+z)}{H_0}D(z), \quad (10)$$

where c is the velocity of light. In a flat universe, $D(z)$ can be expressed as

$$D(z) = \int_0^z \frac{dz}{E(z)}, \quad (11)$$

where $E(z)$ can be worked out with Eq. (6) for the model under consideration.

The chi-square statistic for the Pantheon sample can be constructed as

$$\chi_{\text{SNe}}^2 = \Delta\vec{Y}^T \cdot \mathbf{C}^{-1} \cdot \Delta\vec{Y}, \quad (12)$$

where the residual vector for the SNe Ia data in the Pantheon sample is $\Delta\vec{Y}_i = [Y_i^{\text{obs}} - Y^{\text{th}}(z_i; Y_0, \mathbf{p})]$. The covariance matrix \mathbf{C} of the sample includes the contributions from both the statistical and systematic errors. The nuisance parameter, i.e., the constant term Y_0 is marginalized over with the analytical methodology presented in [31].

3.2. BAO data set

The BAO data extracted from galaxy redshift surveys are also a kind of powerful cosmological probe [32, 33]. The BAO data set used here is a combination of measurements from the 6dFGS at $z_{\text{eff}} = 0.106$ [20], the SDSS DR7 Main Galaxy Sample (MGS) at $z_{\text{eff}} = 0.15$ [21], and the BOSS DR12 at $z_{\text{eff}} = (0.38, 0.51, 0.61)$ [22]. The corresponding measurements are listed in Table 1.

The observable quantities used in the measurements are expressed in terms of the transverse co-moving distance $D_M(z)$, the volume-averaged angular diameter distance $D_V(z)$, the Hubble rate $H(z) \equiv H_0 E(z)$, the sound horizon at the drag epoch r_s , and its fiducial value $r_{s,\text{fid}}$. Following [34], we use the fitting formula of [32] to compute r_s , and $r_{s,\text{fid}}$ is computed with the fiducial cosmology adopted in the paper in which the measurement is reported. In a flat universe, the transverse co-moving

distance $D_M(z)$ equals to the line-of-sight comoving distance $D_C(z)$, which is expressed as,

$$D_C(z) \equiv \frac{c}{H_0}D(z), \quad (13)$$

and c is the speed of light. The volume-averaged angular diameter distance is

$$D_V(z) = \left[\frac{cz}{H_0} \frac{D_M^2(z)}{E(z)} \right]^{1/3}. \quad (14)$$

We employ the BAO data set in the analysis with the chi-squared statistic

$$\chi_{\text{BAO}}^2(p) = [\vec{A}_{\text{th}}(p) - \vec{A}_{\text{obs}}]^T \mathbf{C}^{-1} [\vec{A}_{\text{th}}(p) - \vec{A}_{\text{obs}}], \quad (15)$$

where \mathbf{C}^{-1} is the inverse of the covariance matrix. The BOSS DR12 measurements listed in the last six lines of Table 1 are correlated, and the corresponding covariance matrix is present in Eq.(20) of [34], which is also available from SDSS website¹.

3.3. CMB data set

Observations of the CMB spectra provide another kind of independent test of the existence of dark energy. It is remarkable that the CMB power spectra from the WMAP [35] and Planck projects [19] have provided strong constraints on cosmological parameters. Here, we use the combination of temperature and polarization CMB power spectra from the Planck 2018 release [19], including the likelihoods at multipoles $\ell = 2 - 2508$ in TT, $\ell = 2 - 1996$ in EE, and $\ell = 30 - 1996$ in TE. In practice, different algorithms have been used to estimate the CMB power spectrum, such as Commander[36, 37], SimAll[37] and Pilk[19]. The ‘‘Commander’’ component-separation algorithm is used to estimate the power spectrum over the range $\ell = 2 - 29$ in TT. The ‘‘SimAll’’ approach is used to estimate the power spectrum over the range $\ell = 2 - 29$ in EE. The ‘‘Pilk’’ cross-half-mission likelihood [37] is used to compute the CMB high- ℓ part for TT,TE,EE over the range $30 \leq \ell \leq 2508$ in TT and over the range $30 \leq \ell \leq 1996$ in TE and EE². Hereafter, $\mathcal{L}_{\text{Planck}}$ denotes the likelihood of the Planck data described above.

4. Analysis and Results

4.1. Observational constraints

In our analysis, the total likelihood for parameters is

$$\mathcal{L}(\mathbf{p}) = \prod \mathcal{L}_i, \quad (16)$$

where \mathcal{L}_i means the likelihood of each data set. In the case of using the combination of SNe Ia, BAO and CMB data sets, it takes,

$$\mathcal{L}_{\text{tot}}(\mathbf{p}) = \mathcal{L}_{\text{SNe}} \mathcal{L}_{\text{BAO}} \mathcal{L}_{\text{Planck}} \quad (17)$$

¹https://sdss3.org/science/boss_publications.php

²For more details on the Planck CMB spectrum and likelihood code, see https://wiki.cosmos.esa.int/planckpla/index.php/CMB_spectrum_%26_Likelihood_Code

Table 2: The mean values with 68% confidence limits for model parameters constrained from the Pantheon SNe sample, and from a joint sample of SNe, BAO and CMB data sets, respectively. The scenarios with $\xi = \text{Constant}$ and $\xi(z) = \xi_0 + \xi_z * \frac{z}{1+z}$ are both considered.

Model	Data set	$\Omega_{X,0}$	ω_X	ξ	ξ_0	ξ_z
$\xi = \text{Constant}$	Pantheon	$0.75^{+0.13}_{-0.08}$	$-0.96^{+0.16}_{-0.14}$	$3.42^{+1.22}_{-0.62}$	-	-
$\xi = \text{Constant}$	Pantheon + BAO + CMB	0.67 ± 0.01	-1.12 ± 0.04	3.28 ± 0.15	-	-
$\xi(z) = \xi_0 + \xi_z * \frac{z}{1+z}$	Pantheon	$0.69^{+0.04}_{-0.15}$	$-1.01^{+0.04}_{-0.32}$	-	$3.00^{+0.09}_{-0.78}$	$0.94^{+0.58}_{-1.02}$
$\xi(z) = \xi_0 + \xi_z * \frac{z}{1+z}$	Pantheon + BAO + CMB	0.69 ± 0.01	$-0.99^{+0.03}_{-0.06}$	-	$2.78^{+0.28}_{-1.01}$	$0.93^{+1.56}_{-0.91}$

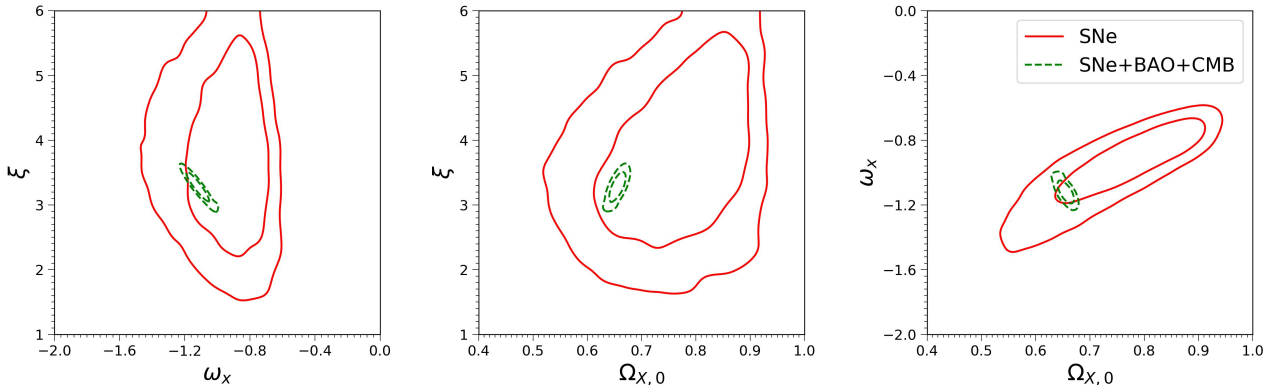


Figure 1: The 2D probability distributions of model parameters in the scenario of $\xi = \text{Constant}$, constrained from the Pantheon SNe sample (red solid lines), and from a joint sample of the SNe, BAO and CMB data (green dotted lines), respectively. The contours correspond to 68% and 95% CLs.

We derive the posterior probability distributions of parameters with Markov Chain Monte Carlo (MCMC) exploration using the May 2020 version of CosmoMC [38]. In the next following analysis, we consider two different treatment schemes for the scaling parameter ξ , i.e., $\xi = \text{Constant}$ and $\xi(z) = \xi_0 + \xi_z * \frac{z}{1+z}$.

The case of $\xi = \text{Constant}$ has been widely studied in the literature [see e.g. 14, 15, 13, 16, 17]. Here we re-explore this scenario with the latest data sets. In addition, the case of $\xi(z)$ is taken into account to explore the possible evolution. We put observational constraints on the model parameters with the recent Pantheon SNe Ia sample, as well as with a combination of the SNe Ia, BAO and CMB data sets, respectively. We present the mean values with 68% confidence limits for the parameters of interest in Table 2 for both scenarios. In the scenario of $\xi = \text{Constant}$, the constraints on $\Omega_{X,0}$, ω_X and ξ from the combining sample are much tighter than those from the single Pantheon SNe Ia sample. The constraints on the parameters ($\Omega_{X,0}$, ω_X , ξ) from the Pantheon SNe sample are consistent with those from the ‘‘Constitution Set’’ SNe sample adopted in [13] at 68% CL. However, the constraints on ($\Omega_{X,0}$, ω_X , ξ) from our combining sample are inconsistent with those from the joint SNe + BAO + CMB sample adopted in [13] at 68% CL, but they are consistent at 95% CL. Moreover, the Λ CDM scenario, i.e., $(\omega_X, \xi) = (-1, 3)$, is accepted by the Pantheon SNe sample at 68% CL, however, it’s ruled out by the combining sample at 99% CL. In the scenario of $\xi(z)$, the constraints on $\Omega_{X,0}$ and ω_X from the combining sample are much tighter than those from the Pantheon SNe sample, but the constraint precisions on ξ_0 and ξ_z from the combining sample do not have significant improvements compared with those from the single Pantheon SNe sample. The Λ CDM scenario, i.e.,

$(\omega_X, \xi_0, \xi_z) = (-1, 3, 0)$, is accepted by the Pantheon SNe sample but ruled by the combining sample at 68% CL, nevertheless, it’s accepted by the combining sample at 95% CL. Then, we pay attention to the constraints on the parameter ξ_z which indicates the degree of temporal evolution of the scaling parameter ξ . The mean values with 68% confidence limits for the parameters ξ_z are $\xi_z = 0.94^{+0.58}_{-1.02}$ from the Pantheon SNe sample and $\xi_z = 0.93^{+1.56}_{-0.91}$ from the combining sample. It implies that the Pantheon SNe sample cannot distinguish between the evolving and non-evolving scenarios, and the combining sample supports the time-evolving scenario at 68% CL.

The two-dimensional (2D) contours for the model parameters of interest are presented in Fig. 1 for the scenario of $\xi = \text{Constant}$ and in Fig. 2 for the scenario of $\xi(z)$. From Fig. 1, one also can see that the constraints from the combining sample are much more restrictive than those from the Pantheon SNe sample, though there are degeneracies between some parameters. The $\omega_X - \xi$ plane does not have significant degeneracy from the Pantheon SNe sample, but displays a negative correlation from the combining sample. The $\Omega_{X,0} - \xi$ plane demonstrates a positive correlation from both the single Pantheon SNe sample and the combining sample. Especially, the $\Omega_{X,0} - \omega_X$ plane displays a positive correlation from the Pantheon sample, conversely, a negative correlation from the combining sample. From Fig. 2, one can find out that the contours constrained from the combining sample shrink significantly compared with those from the Pantheon SNe sample except for the last panel, i.e., the $\xi_0 - \xi_z$ plane. It implies that the addition of the BAO and CMB data sets cannot greatly improve the constraint precisions on ξ_0 and ξ_z .

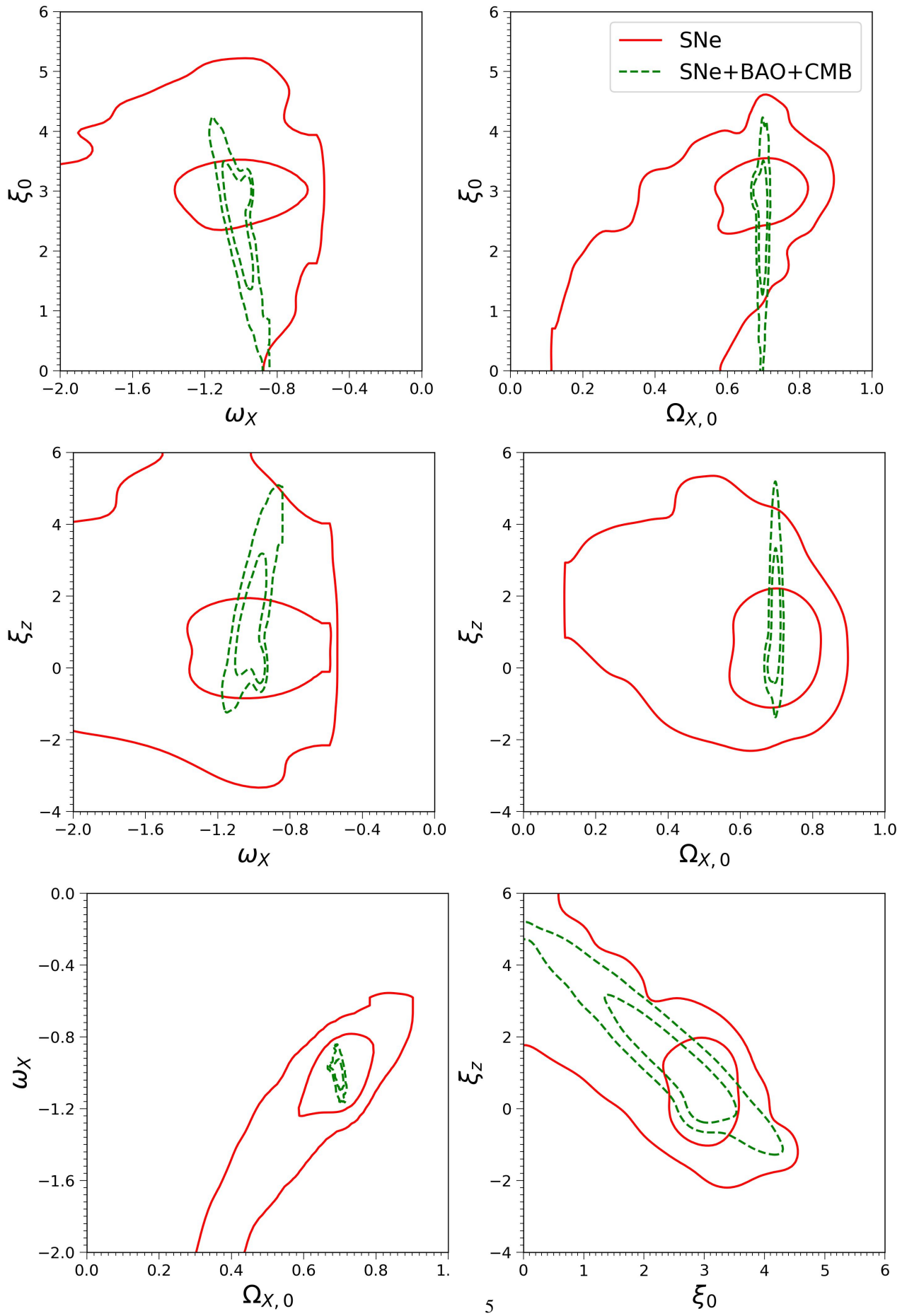


Figure 2: The 2D contours of parameters in the scenario of $\xi(z) = \xi_0 + \xi_z * \frac{z}{1+z}$. The implications of line styles are the same as those in Fig.1.

Table 3: We list the natural logarithm of the Bayesian evidences $\ln B_i$ and the Bayes factors $\ln B_{i,0}$ from the joint sample of SNe+BAO+CMB, where the subscript “0” denotes the Λ CDM model.

Model	$\ln B_i$	$\ln B_{i,0}$
Λ CDM	-1940.80	0
$\rho_X \propto \rho_m a^\xi$ with $\xi = \text{Constant}$	-2022.22	-81.42
$\rho_X \propto \rho_m a^\xi$ with $\xi(z) = \xi_0 + \xi_z * \frac{z}{1+z}$	-2030.04	-89.24

4.2. Model selection statistics

In the framework of Bayes’ theorem, the probability that the model M_i is true can be estimated with

$$P(M_i | D) = \frac{P(D | M_i) P(M_i)}{P(D)}, \quad (18)$$

where $P(M_i | D)$ is the posterior probability, D denotes the observational data, $P(M_i)$ is a prior probability in the model M_i , and $P(D)$ is the normalization constant. In addition, $P(D | M_i)$ is the so-called Bayesian evidence [39, 40], which can be written as

$$P(D | M_i) = \int P(D | \bar{\theta}, M_i) P(\bar{\theta} | M_i) d\bar{\theta}, \quad (19)$$

where $P(D | \bar{\theta}, M_i)$ is the likelihood function under the model M_i , and $P(\bar{\theta} | M_i)$ is the prior probability for parameter $\bar{\theta}$ under the model M_i . Hence, calculating the Bayesian evidence requires the evaluation of an integral over the entire likelihood function and the prior distributions of model parameters. When comparing two models, e.g., M_i versus M_j , the Bayes factor

$$B_{ij} = \frac{P(D | M_i)}{P(D | M_j)}, \quad (20)$$

which is defined as the ratio of the Bayesian evidences of two models can be employed as a judgment criterion, where the Bayes factor $B_{ij} > 1$ (i.e., $\ln B_{ij} > 0$) means that the observational data prefer M_i to M_j , and $B_{ij} < 1$ implies that M_j is preferred [41].

To compare the phenomenological models under consideration with the Λ CDM model, we calculate the values of Bayesian evidence for each model, where the code **MCEvidence** [42] which is a popular python package to compute the Bayesian evidence is adopted here, and the observational data correspond to the joint sample of SNe, BAO and CMB data. In Table 3, we show the natural logarithm of the Bayesian evidence for each model, $\ln B_i$, as well as the natural logarithm of the Bayes factor, $\ln B_{i,0}$, where the subscript “0” denotes the Λ CDM model. It turns out that the Λ CDM model is most supported by the joint sample, since $B_{1,0}$ and $B_{2,0}$ are both smaller than 1, where the subscripts “1” and “2” denote the scenarios with a constant ξ and a variable $\xi(z)$, respectively. In addition, $B_{1,2} = B_1/B_2$ is bigger than 1, so the scenario with a constant ξ is more competitive than the one with a variable ξ_z .

5. Summary and conclusions

We have concentrated on a kind of phenomenological model of cosmology, where the assumption of $\rho_X \propto \rho_m a^\xi$ is adopted.

As a key parameter, the scaling parameter ξ reveals the severity of the coincidence problem, where the particular values $\xi = 3$ and $\xi = 0$ correspond to the Λ CDM scenario and the self-similar solution without coincidence problem, respectively. Besides the scheme of assuming $\xi = \text{Constant}$, we have also considered the scenario with a variable $\xi(z) = \xi_0 + \xi_z * \frac{z}{1+z}$ to explore the possible evolution. The observational constraints on the model parameters are conducted with both the single Pantheon SNe Ia sample and a joint sample of SNe, BAO and CMB data sets, where the CMB power spectrum data are from the Planck 2018 final analysis, and the BAO data are from the measurements of 6dFGS, SDSS DR7 MGS, and BOSS DR12.

The main conclusions can be summarized as follows: (i) In the case of $\xi = \text{Constant}$, the Λ CDM scenario, i.e., $(w_X, \xi) = (-1, 3)$, is accepted by the Pantheon SNe sample and by the joint sample at 68% CL and 95% CL, respectively. Moreover, in the case of a variable $\xi(z)$, the Λ CDM scenario, i.e., $(w_X, \xi_0, \xi_z) = (-1, 3, 0)$, is also accepted by the Pantheon SNe sample and by the joint sample at 68% CL and 95% CL, respectively. (ii) According to the observational constraints on the model parameters, the Pantheon SNe sample cannot distinguish between the scenarios of a constant ξ and a variable $\xi(z)$ at 95% CL because of $\xi_z \in [-2.60, 5.23]$ at 95% CL; moreover, the joint sample also cannot distinguish whether the scaling parameter ξ is variable or not at 95% CL because of $\xi_z \in [-0.67, 4.40]$ at 95% CL. (iii) According to the Bayesian evidences calculated from the joint sample, we find out that the Λ CDM model is most supported by the joint sample; furthermore, the joint sample prefers the scenario with a constant ξ to the one with a variable $\xi(z)$. (iv) The inclusion of the BAO and CMB data sets just can provide very limited improvements on constraining ξ_0 and ξ_z in the scenario of $\xi(z)$, but it has significantly reduced the allowed regions of other parameters. Thus, to diagnose the evolution of the scaling parameter ξ more robustly, it seems to be quite necessary to explore other probes which can supply more efficient improvements on constraining ξ_0 and ξ_z .

6. acknowledgments

This work has been supported by the National Natural Science Foundation of China (Nos. 11988101, 11633001, 11920101003, 11703034, 11773032 and 11573031), the Strategic Priority Research Program of the Chinese Academy of Sciences (No. XDB23000000), the Interdiscipline Research Funds of Beijing Normal University, and the NAOC Nebula Talents Program.

Note added. The data underlying this article will be shared on reasonable request to the corresponding author.

References

- [1] P. Bull, et al., Physics of the Dark Universe **12** (2016) 56.
- [2] J. S. Bullock, M. Boylan-Kolchin, ARAA **55** (2017) 343.
- [3] S. Weinberg, Rev. Mod. Phys **61** (1989) 1.
- [4] S. M. Carroll, W. H. Press, E. L. Turner, ARAA **30** (1992) 499.
- [5] S. Weinberg, arXiv:astro-ph/0005265.
- [6] A. Vilenkin, arXiv:hep-th/0106083.

- [7] J. Garriga, M. Livio, A. Vilenkin, Phys. Rev. D **61** (1999) 023503.
- [8] J. Garriga, A. Vilenkin, Phys. Rev. D **64** (2001) 023517.
- [9] E. J. Copeland, M. Sami, S. Tsujikawa, Int. J. Mod. Phys. D **15** (2006) 1753.
- [10] L. Amendola, arXiv:astro-ph/9908023v1.
- [11] G. Caldera-Cabral, R. maartens, A. Urena-Lopez, arXiv:0812.1827v2.
- [12] N. Dalal, et al., Phys. Rev. Lett. **87** (2001) 141302.
- [13] Y. Chen, et al., Astrophys. J. **711** (2010) 439.
- [14] D. Pavón, S. Sen, W. Zimdahl, JCAP **5** (2004) 009.
- [15] Z. K. Guo, N. Ohta, S. Tsujikawa, Phys. Rev. D **76** (2007) 023508.
- [16] S. Cao, N. Liang, Z.-H. Zhu, Mon. Not. R. Astron. Soc. **416** (2011) 1099.
- [17] M.-J. Zhang, W.-B. Liu, EPJC **74** (2014) 2863.
- [18] D. Scolnic, et al., Astrophys. J. **859** (2018) 101.
- [19] N. Aghanim, et al., *a* **641** (2020) A6. arXiv:1807.06209.
- [20] F. Beutler, et al., Mon. Not. R. Astron. Soc. **416** (2011) 3017.
- [21] A. J. Ross et al., Mon. Not. R. Astron. Soc. **449** (2015) 835.
- [22] S. Alam, et al., Mon. Not. R. Astron. Soc. **470** (2017) 2617.
- [23] D. Branch, D. L. Miller, APJL **405** (1993) L5.
- [24] A. G. Riess, W. H. Press, R. P. Kirshner, APJL **438** (1995) L17.
- [25] A. V. Filippenko, ASSL **332** (2005) 97 [arXiv:astro-ph/0410609].
- [26] J. Guy, et al., Astron. Astrophys. **443** (2005) 781.
- [27] J. Guy, et al., Astron. Astrophys. **466** (2007) 11.
- [28] A. Conley, et al., Astrophys. J. **681** (2008) 482.
- [29] M. Betoule, et al., Astron. Astrophys. **568** (2014) A22.
- [30] R. Kessler, D. Scolnic, Astrophys. J. **836** (2017) 56.
- [31] R. Giotri, et al., JCAP **03** (2012) 027.
- [32] D. J. Eisenstein, W. Hu, Astrophys. J. **496** (1998) 605
- [33] D. J. Eisenstein, et al., Astrophys. J. **633** (2005) 560.
- [34] J. Ryan, Y. Chen, B. Ratra, Mon. Not. R. Astron. Soc. **488** (2019) 3844
- [35] G. Hinshaw, et al., Astrophys. J. Suppl. **208** (2013) 19.
- [36] Y. Akrami, et al., Astron. Astrophys. **641** (2020) 74.
- [37] N. Aghanim, et al., Astron. Astrophys. **641** (2020) 92.
- [38] A. Lewis, S. Bridle, Phys. Rev. D **66** (2002) 103511.
- [39] R. Trotta, Contemporary. Physics. **49** (2008) 71.
- [40] G. Efstathiou, Mon. Not. R. Astron. Soc. **388** (2008) 1314.
- [41] M. Szydlowski, et al., Eur. Phys. J. C **75** (2015) 5.
- [42] A. Heavens, et al., arXiv:1704.03472.